THE JOURNAL OF PHYSICAL CHEMISTRY B

ARTICLE

pubs.acs.org/JPCB

Combined Use of Replica-Exchange Molecular Dynamics and Magic-Angle-Spinning Solid-State NMR Spectral Simulations for Determining the Structure and Orientation of Membrane-Bound Peptide

Keisuke Ikeda,[†] Tomoshi Kameda,[‡] Erisa Harada,[†,§] Hideo Akutsu,[†] and Toshimichi Fujiwara*[,†]

[†]Institute for Protein Research, Osaka University, 3-2 Yamadaoka, Suita 565-0871 Japan

[‡]Computational Biology Research Center, Advanced Industrial Science and Technology, 2-4-7 Aomi, Koto-ku, Tokyo 135-0064, Japan

Supporting Information

ABSTRACT: We report an approach to determining membrane peptides and membrane protein complex structures by magic-angle-spinning solid-state NMR and molecular dynamics simulation. First, an ensemble of low energy structures of mastoparan-X, a wasp venom peptide, in lipid bilayers was generated by replica exchange molecular dynamics (REMD) simulation with the implicit membrane/solvent model. Next, peptide structures compatible with experimental $^{13}C^{\alpha}$, C^{β}, and C' chemical shifts were selected from the ensemble. The $^{13}C^{\alpha}$ chemical shifts alone were sufficient for the selection with backbone rmsd's of ~0.8 Å from the experimentally determined structure. The dipolar couplings between the peptide protons and lipid $^{2}H/^{31}P$ nuclei were obtained from the ^{13}C-observed $^{2}H/^{31}P$-selective ^{1}H-demagnetization experiments for selecting the backbone and side chain structures relative to the membrane. The simulated structure agreed with the experimental one in the depth and orientation. The REMD simulation can be used for supplementing the limited structural constraints obtainable from the solid-state NMR spectra.

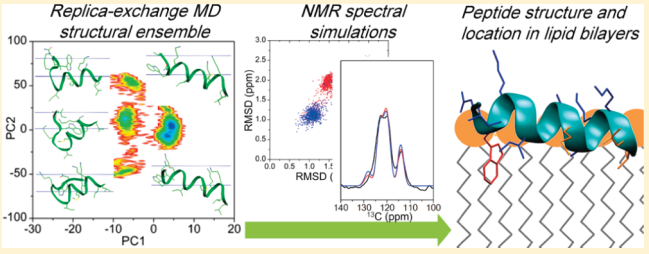

INTRODUCTION

Membrane proteins and peptides are involved in diverse biological functions.[1,2] Native lipid bilayer environments are critical for exerting their functions. Magic-angle-spinning (MAS) solid-state NMR spectroscopy is suitable for studying their structures, dynamics, and interactions with lipid molecules in near-native lipid bilayer environments such as liposomes.[1,2] However, the determination of molecular structures of membrane-associated proteins and peptides by solid-state NMR is still difficult. The acquisition of structural constraints from uniformly isotope $^{13}C,^{15}N$-labeled proteins is hampered by low spectral resolution especially for large membrane protein systems. Site-specific isotope labeling enables distances and torsion angle measurements for simplified spectra. However, a small amount of information solely for the labeled sites limits the determination of a whole molecular structure. So far, protein structures are determined by solid-state NMR mainly (1) for microcrystals and amyloid fibrils showing narrow peaks due to homogeneous molecular structures and (2) for small peptides having a small number of nuclear spins (Protein Data Bank accessed in April 2010).

Molecular dynamics (MD) simulation, on the other hand, has been widely used for studying proteins in the membranes. Especially advanced sampling techniques such as replica exchange molecular dynamics (REMD) allow enhanced conformational sampling in rugged free energy landscapes.[3] Im et al. demonstrated that REMD simulation successfully predicted conformations of small membrane proteins and folding/insertion processes of designed peptides into membranes.[4,5] To save computational cost, they treated membranes and bulk water as continuum medium using an implicit membrane/solvent model, where the electrostatic and nonelectrostatic parts of solvation energy were expressed by the generalized Born energy and the accessible surface area model, respectively.[6,7]

Nevertheless, it is difficult to predict structures of membrane proteins accurately only by the MD simulations without experimental information. Combination of NMR with computer simulation is promising for determining structures of proteins and peptides using limited experimental data. Shen et al. determined protein structures by using only backbone and C^{β} chemical shifts in combination with fragment assembly.[8] Molecular dynamics simulations were performed under conformational restraints obtained from solid-state NMR to determine the backbone structure of membrane proteins in lipid membranes.[9] Chen et al. refined solution NMR structures of proteins with sparse distance constraints by REMD simulations with the implicit solvent water model.[10] However, REMD with implicit membrane/solvent has not been used for the structure determination of membrane proteins with limited NMR structural data.

Received: June 6, 2011
Published: June 13, 2011

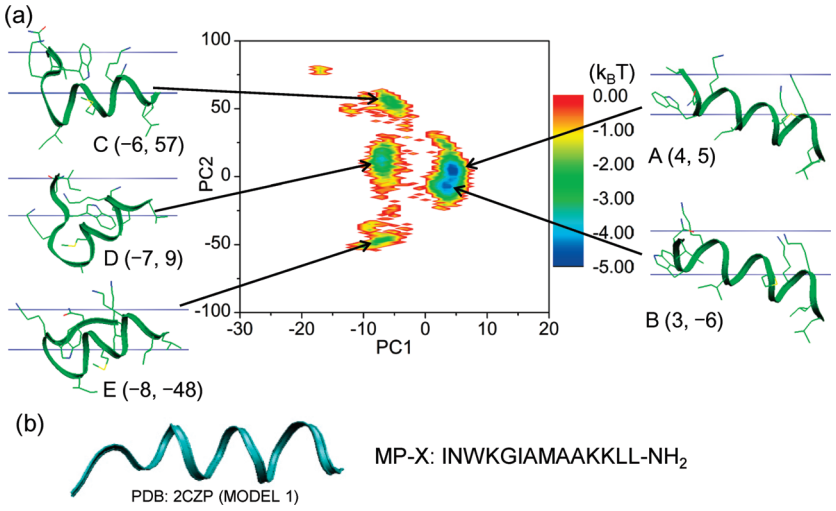

Figure 1. Structural ensemble of MP-X. (a) Free-energy landscape of MP-X structures at 300 K obtained by the REMD simulation for the implicit membrane model. The two-dimensional space was spanned by the first and second principal components. The color scale shows the free energy (k_BT unit) estimated from the population of the structures at (PC1, PC2). The representative structures at the local minimum of free energy basins A−E are shown with the upper and lower limits of the water−membrane interface region indicated by blue lines. (b) The amino acid sequence and the NMR backbone structure of MP-X (PDB: 2CZP).[14]

Previously, our group presented a method for automatic chemical shift assignment and backbone structure determination of a uniformly ^{13}C-labeled membrane-bound peptide: simulated-annealing spectral fitting for MAS NMR by molecular dynamics calculation with simplified potentials.[11] In this study, we report a method for determining structures of membrane peptides and membrane protein complexes by MAS solid-state NMR and advanced molecular dynamics simulation. First, an ensemble of low-energy structures is generated mainly by REMD simulation with the implicit membrane/solvent model. We select structures from the ensemble using chemical shifts and dipolar couplings. The chemical shifts are predicted from the structures in the ensemble to compare with the experimental shifts. The dipolar couplings are obtained from the previous experiments for ^{13}C-observed ^{2}H/^{31}P-selective ^{1}H-demagnetization (COXSHD). The signal intensities of COXSHD depend on distances between the peptide protons and lipid ^{2}H/^{31}P nuclei. We simulate the spectra to obtain structural constraints even from the solid-state NMR spectra containing many overlapped signals. A wasp venom peptide, mastoparan-X (MP-X), in phospholipid bilayers is analyzed as a model system for evaluating our procedure (Figure 1b),[12,13] because the backbone structure and the location of MP-X in phospholipid bilayers were previously determined by intensive MAS solid-state NMR experiments.[14,15]

EXPERIMENTAL SECTION

REMD in the Implicit Membrane/Solvent. REMD simulations were performed as previously described by Im and Brooks.[4,5] The generalized Born model with a switching function (GBSW) module in the CHARMM program (c35b2) was used for implicit membrane and solvent.[6,7,16] A time step of 2 fs and all-atom parameter set PARAM22 including CMAP were used.[17] The SHAKE algorithm was applied to covalent bonds connected to hydrogen atoms.[18] Cutoff distances for nonbonded interactions and GB terms were set at 20 Å. A smoothing length of 0.6 Å at the dielectric boundary was used with 24 radial integration points and 38 angular integration points. Langevin dynamics with a friction coefficient of 5.0 ps^{-1} was used. We used the surface tension coefficient of 0.04 kcal/mol Å^2 for the accessible surface area model. The imaginary planar membrane was set perpendicular to the z_{IM} axis. The membrane consisted of the hydrophobic core having 38-Å thickness with 5-Å smoothing regions which represented the water−membrane interfaces.

The replica temperatures were kept by a Nosé−Hoover thermostat.[19] An exchange of replicas was attempted every 1 ps. The average pairwise exchange rate was estimated at 65%. The MMTSB toolset was used for the control of the REX simulations.[20] A fully extended structure and a helical structure determined by solid-state NMR experiments (PDB: 2CZP, MODEL 1) were adopted as initial structures for the simulations.[14] The molecular dynamics was calculated for 16 and 12 ns beginning from the extended and helical MP-X, respectively. The 10-ns runs were also performed for the two initial conformations without the membranes. The secondary structure contents were analyzed using STRIDE.[21]

Principal Component Analysis (PCA). We performed PCA for the analysis of the energy landscape following the procedure reported previously.[22,23] First, we selected 512 000 configurations from the snapshots of all replicas for the simulation of MP-X (initial structure: extended peptide) with the implicit membranes. These structures were superimposed on a reference structure (PDB: 2CZP, MODEL 1). The variance−covariance matrix of the ensemble was diagonalized to obtain eigenvectors and eigenvalues which represented the standard deviations of the conformational distribution along the PC axes. The conformations of MP-X with implicit membranes at 300 K from the 7001−16000-ps simulation were projected onto the two-dimensional space spanned by the first and second principal axes, PC1 and PC2. The cumulative contribution of two PCs is about 98%, which showed the two axes can primarily characterize the structure for the cluster analysis.

Chemical Shift Prediction. Chemical shifts (C^{α}, C^{β}, and C') were predicted from the simulated conformations using the SHIFTX version 1.1 and SPARTA version 1.01 programs.[24,25]

COXSHD Spectral Fitting. The details of the COXSHD experiments were described in a previous report.[14] The signal

Table 1. Parameters for MP-X Structures at the Basins in the PC Space

	(PC1, PC2)[a]	ΔG (k_BT)	backbone rmsd[b] (Å)	C^α chemical shift rmsd (SHIFTX)[b] (ppm)	C^α chemical shift rmsd (SPARTA)[b] (ppm)
A	(4, 5)	−4.80	1.64 ± 0.21	1.55 ± 0.21	1.87 ± 0.23
B	(3, −6)	−4.48	0.76 ± 0.22	1.11 ± 0.17	1.16 ± 0.21
C	(−6, 57)	−3.26	4.58 ± 0.26	2.06 ± 0.14	2.03 ± 0.13
D	(−7, 9)	−3.66	4.41 ± 0.12	2.34 ± 0.12	2.36 ± 0.11
E	(−8, −48)	−2.89	4.05 ± 0.12	1.90 ± 0.18	2.07 ± 0.20

[a] PC coordinates at the minimum in each basin. [b] Statistics for the structures around the minimum, (PC1 ± 1, PC2 ± 4).

intensities of the COXSHD spectra depend on the distance d_{H-X} between a $^2H/^{31}P$ spin and a ^1H spin attached to ^{13}C. This distance dependence was approximately expressed as

$$M_0 G_X(d_{H-X}) = M_0 \, exp\left\{-\frac{1}{2}\left(\frac{d_{H-X}}{d_{X0}}\right)^2\right\} \quad (1)$$

with the initial ^1H magnetization M_0, and d_{X0} = 0.18 nm for ^2H and 0.30 nm for ^{31}P. The control distance for the depolarization d_{X0} was estimated from numerical simulations of ^1H depolarization for the two-spin systems $^2H-^1H$ and $^{31}P-^1H$.[15] The polarization was calculated as a function of τ_{dp} for d_{H-X} in the range 0.15−0.55 nm. The parameter d_{X0} was obtained by fitting the calculated depolarization magnitude to eq1 as a function of d_{H-X}. Here τ_{dp} was selected to maximize the depolarization at each distance.

The depolarization of a ^1H at $\mathbf{r} = (x, y, z)$ in a lipid bilayer was given by

$$f_X(\mathbf{r}) = \frac{M_0}{C_N}\sum_{i=1}^{N} G_X(|\mathbf{r} - \mathbf{r}_i|)$$

where $\mathbf{r}_i = (x_i, y_i, z_i)$, $i = 1-N$, gives the coordinates of the X spin in a bilayer consisting of 72 dipalmitoylphosphatidylcholine (DPPC) molecules and 2094 water molecules equilibrated by molecular dynamics simulation under CHARMM force field (PARAM27).[26] This model assumes that the ^1H depolarization at $\mathbf{r}$ is determined by the density of the X spin with the radius d_{X0}. The normalization constant C_N assures $f_X(\mathbf{r}) \le M_0$.

We assume that the X spins were uniformly distributed on the xy-plane which is parallel to the bilayer surface. Therefore, we can make the depolarization depend only on the bilayer depth z for a ^1H spin, when ^1H spin at $\mathbf{r}$ is replaced by the average over the membrane plane.

$$f_X(z) \approx \frac{M_0 2\pi {d_0}^2}{C_N L^2}\sum_{i=1}^{N} G_X(z - z_i)$$

Here L^2 denotes the area of the membrane plane. The resulting ^1H-demagnetization functions $f_{^2H}(z)$ and $f_{^{31}P}(z)$ are shown in Figure 3b.

The ^{13}C spectrum $S_X(\omega_z)$ for the X-selective depolarization was computed as a sum of signals each of which is defined by intensity $f_X(z_j)$, chemical shift δ_j, line width $\Delta_{1/2}$ for ^{13}C nucleus j, and the number of ^{13}C nuclei M in MP-X:

$$S_X(\omega_z) = C_X\sum_{j=1}^{M}\eta_j f_X(z_j)\, exp\left\{-\left(\frac{\omega_z - \delta_j}{\Delta_{1/2}/2\sqrt{ln\,2}}\right)^2\right\}$$

Here, efficiencies of the magnetization transfer η_j from ^1H to ^{13}C by Lee−Goldburg cross-polarization (LGCP) were 0.68, 0.63, and 0.59 for CH, CH_2, and CH_3, respectively. The coefficient C_X was determined at each structure and position of MP-X to fit the simulated spectra to the experimental ones.

RESULTS

Generation of MP-X Structure in Implicit Membranes by REMD Simulation. REMD simulation of MP-X was initiated from a fully extended or an α-helical conformation of the peptide placed in the xy-plane at z_{IM} = 19.0 Å, the center of membrane/solvent interface (16.5 ≤ z_{IM} ≤ 21.5 Å). The temperatures of 32 replicas were distributed in the range 300−800 K. The time courses of the location in z_{IM} (Figure S1a,b in the Supporting Information), potential energy (Figure S1c,d in the Supporting Information), backbone root-mean-square deviation (rmsd) from the NMR structure (Figure S1e,f in the Supporting Information), and secondary structure (Figure S1g,h in the Supporting Information) at 300 K were monitored. During the simulation, the peptide resided in the interfacial region of the implicit membranes, where the dielectric constant was smoothly increased from the low dielectric hydrophobic membrane core region (z_{IM} < 16.5 Å) to the high dielectric aqueous region (z_{IM} > 21.5 Å). We observed neither deep insertion of the peptide backbone into the membrane core like a transmembrane helix nor the dissociation from the membrane into the aqueous phase. The potential energy of the system gradually decreased from 0 to −64 (±11) kcal/mol during the first 1-ns simulation. The peptide conformation changed from the extended to α-helix-rich structures (Figure S1g in the Supporting Information). Figure S1e,f in the Supporting Information shows the rmsd of backbone atoms between the simulated structure and the membrane-bound MP-X structure previously determined by the MAS solid-state NMR (Figure 1b).[14] The structures with low rmsd (<1.0 Å) at 300 K demonstrated that the REMD simulation with the implicit membrane/solvent explored the conformational space including the NMR structures. In contrast, MP-X did not form α-helix-rich conformations under the aqueous environment (Figure S2e,f in the Supporting Information). The average α-helix content at 300 K was 0.39, while that was 0.72 under the membrane environment. The backbone rmsd for the aqueous system also did not decline to a level under 1.0 Å, unlike that for the membrane system (Figure S2c,d in the Supporting Information). These results clearly show that the membranes strongly induced α-helical structures consistent with experimental observations.[14] It should be noted that initial structure, extended or helical structure, did not affect the conformations at simulation time longer than 7000 ps regardless of the environment as shown by Figures S1and S2 in the Supporting Information, suggesting that the 10-ns run per replica, a total of 320-ns run, was sufficiently long for the convergence of the simulations.

The atomic coordinates in the trajectory were subjected to PCA for classifying major conformational states.[22] The free

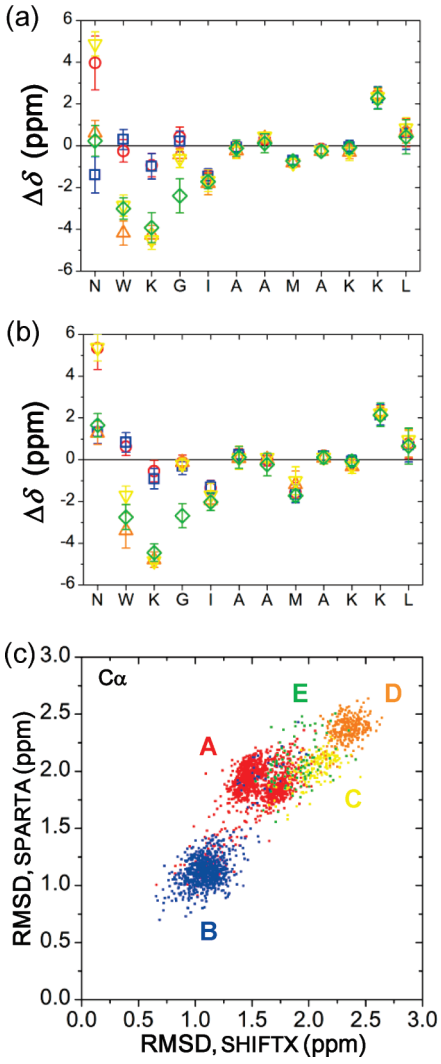

Figure 2. (a, b) Difference ($\Delta\delta = \delta_{obs} - \delta_{pred}$) between the observed ($\delta_{obs}$) and predicted ($\delta_{pred}$) chemical shifts for C^{α} nuclei in residues 2−13. The chemical shifts were calculated using the programs SHIFTX (a) and SPARTA (b). The differences for structures are shown with red circles for basin A, blue squares for B, yellow inverted triangles for C, orange triangles for D, and green diamonds for E. (c) The rmsd between the observed and predicted chemical shifts for C^{α} in residues 2−13 at basins A−E. The structures were taken in the region of (PC1 ± 1, PC2 ± 4) around each minimum.

energy (k_BT unit) was calculated using the number of occurrences of the structures at (PC1, PC2) in the two-dimensional space spanned by the first and second principal components. The free energy landscape for 9000 structures in 7001−16 000 ps at 300 K is shown in Figure 1a. Five local minimal basins were found: A, (PC1, PC2) = (4, 5); B, (3, −6); C, (−6, 57); D, (−7, 9); E, (−8, −48) (Table 1). The representative molecular structures are also depicted. In the most stable basin, A ($\Delta G = -4.80k_BT$), the peptide formed the α-helix from N2 to L13. In the second most stable basin, B ($\Delta G = -4.48k_BT$), the peptide also formed the α-helix-rich conformations from W3 to L13 with the N-terminal two residues forming the extended structures. The rmsd's of the backbone structures at basins A and B from that determined by the NMR were 1.64 ± 0.21 and 0.76 ± 0.22 Å, respectively.[14] The other three basins (C, D, and E, $\Delta G > -3.70k_BT$) gave the flexible backbone conformations especially for the N-terminal residues, I1−G5. Although the backbone rmsd's in these basins from the NMR structure are larger than 4 Å, the ensemble containing these less α-helical structures at 300 K does not conflict with the experimental results for circular dichroism (CD) spectroscopy.[12] The α-helix content of MP-X bound to phosphatidylcholine liposomes at a room temperature was roughly estimated at 0.6 from the ellipticity of CD at 222 nm, which is consistent with the average helix content of 0.72 in the present simulation.

Selection of Backbone Structures from the Ensemble by Chemical Shifts. In the previous section, we showed that REMD simulation could generate membrane-bound MP-X structures consistent with the solid-state NMR structure. Here, we sifted out structures from the ensemble through chemical shifts reflecting local structural environments. The programs SHIFTX and SPARTA empirically compute the protein chemical shifts on the basis of the protein structure−chemical shift database (Biological Magnetic Resonance Data Bank) (http://www.bmrb.wisc.edu/) and physicochemical theories such as ring currents and hydrogen bonds.[24,25] We calculated the differences $\Delta\delta$ between the experimental isotropic chemical shifts (BMRB entry: 10001) and the calculated shifts that were predicted by SHIFTX and SPARTA for the MP-X structures in all the basins at 300 K. Chemical shift rmsd's were defined as

$$rmsd = \sqrt{\frac{1}{N}\sum_{i=1}^{N}(\delta_{obs,i} - \delta_{pred,i})^2}$$

where N, $\delta_{obs,i}$, and $\delta_{pred,i}$ denote the total number of nuclei ($^{13}C^{\alpha}$, $^{13}C^{\beta}$, and $^{13}C'$), observed shifts of the nucleus i, and predicted shifts of the nucleus i, respectively. We did not include the chemical shifts of the terminal residues, I1 and L14, and ^{15}N nuclei because of the lower reliability of the prediction. The $\Delta\delta$ values and rmsd's for $^{13}C^{\alpha}$ (Figure 2), $^{13}C^{\beta}$, and $^{13}C'$ (Figure S3 in the Supporting Information) of the structures at PCA basins are shown. Because residues I6−L13 at all the basins formed the α-helical structures, the difference in $\Delta\delta$ between the basins was smaller than 0.5 ppm. The residues N2−G5, however, had a much larger difference, indicating structural heterogeneity. The structures at basin B with the smallest backbone rmsd were discriminated from those at the other basins by the smallest $\Delta\delta$, and the sum of chemical shift rmsd's for C^{α}, C^{β}, and C'. Specifically, basin B showed chemical shift rmsd's of 1.11 (SHIFTX) and 1.16 ppm (SPARTA) for C^{α} (Table 1). The rms prediction errors for C^{α} by these programs were reported to be about 1.2 ppm for crystalline and membrane proteins and about 1.0 ppm for proteins in solution.[27] Therefore, basin B gave the structures that best explained the experimental chemical shifts. However, we could not select a unique structure from the chemical shift optimization only by C^{β} and/or C' because of the overlap of the structures in the two-dimensional rmsd plot (Figure S3 in the Supporting Information). This indicates that the prediction of C^{α} chemical shifts was most sensitive in selecting the correct conformations from the ensemble. The narrow average ^{13}C line width of ∼0.7 ppm excluding J_{C-C} couplings suggests that MP-X fell into the global minimum energy state with the homogeneous secondary structures at a low temperature of 253 K for the NMR experiments.[14] This is best exemplified by the $^{13}C^{\alpha}$ resonance of N2: the predicted chemical shift for all the basins gave a distribution over a range of 7 ppm but the observed line width of ∼0.7 ppm was much smaller.

Table 2. Simulated and Experimental Interatomic Distances (Å) for MP-X

	A	B	C	D	E	exptl[a]
I1[^{13}C′]−G5[^{15}N]	4.6 ± 0.7	6.1 ± 0.5	11.2 ± 0.4	8.9 ± 0.4	9.3 ± 0.6	6.0 ± 0.4[b]
G5[^{13}C′]−A8[$^{13}C^{\beta}$]	4.3 ± 0.2	4.3 ± 0.2	4.3 ± 0.2	4.4 ± 0.2	4.6 ± 0.4	4.2 ± 0.1[c]
A7[^{13}C′]−A10[$^{13}C^{\beta}$]	4.3 ± 0.2	4.3 ± 0.2	4.3 ± 0.2	4.3 ± 0.3	4.4 ± 0.3	4.2 ± 0.1[b]
A10[^{13}C′]−L13[^{15}N]	3.9 ± 0.2	3.9 ± 0.2	3.9 ± 0.2	3.9 ± 0.2	3.9 ± 0.2	4.2 ± 0.1[c]
A10[^{13}C′]−L14[^{15}N]	4.2 ± 0.2	4.2 ± 0.2	4.2 ± 0.2	4.2 ± 0.2	4.2 ± 0.2	4.4 ± 0.1[c]

[a] Experimental distances from ref 14. [b] Distances obtained by REDOR experiments. [c] Distances obtained by RR experiments.

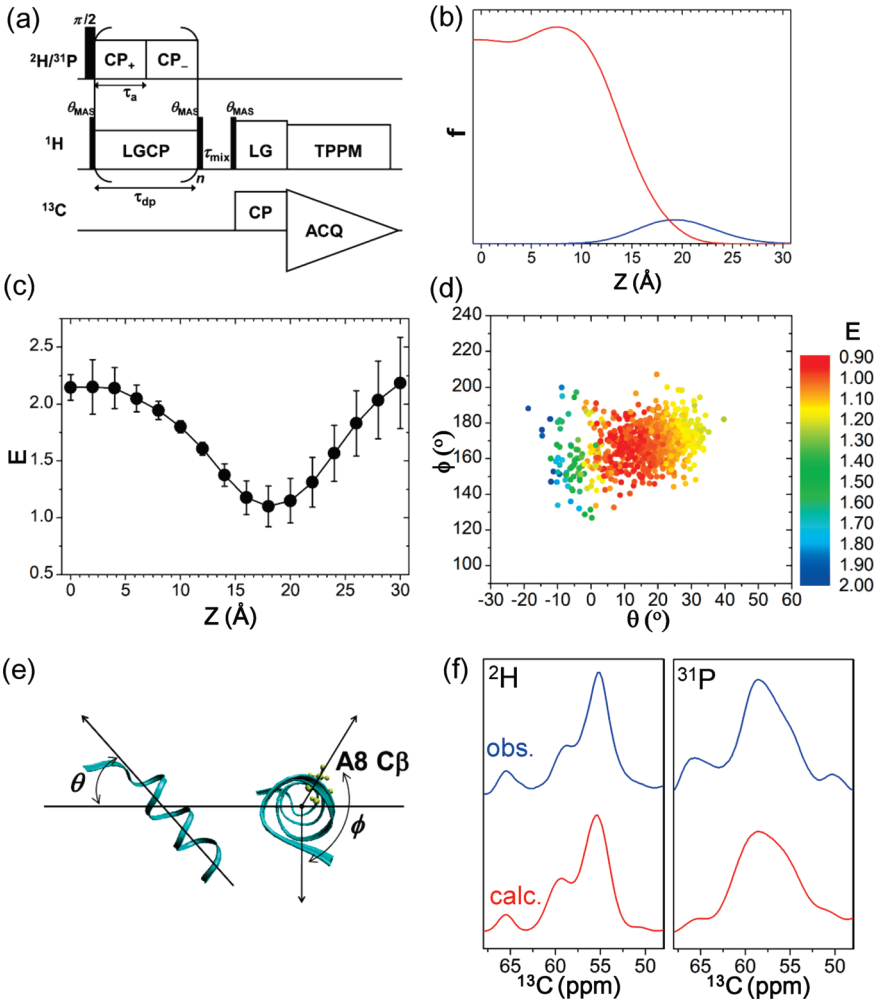

Figure 3. (a) Pulse scheme for ^{13}C observation of ^{2}H/^{31}P-selective ^{1}H-demagnetization under MAS. (b) ^{2}H- and ^{31}P-selective ^{1}H depolarization, $f_{2H}(z)$ (red) and $f_{31P}(z)$ (blue) as a function of depth z. (c) Target function for spectral fitting E depending on the depth of the backbone center of mass at the basin B. The C^{α} spectral region, 45−68 ppm, was used for the spectral simulation. The spectral fit was optimized at z = 18 Å. (d) Dependence of E on the simulated orientations (θ, ϕ) of the peptide at z = 18 Å. (e) The helix tilt angle θ and rotation angle ϕ. (f) Observed (blue) and simulated (red) CO^{2}HSHD and CO^{31}PSHD spectra. The simulated spectra obtained from the structure at z = 18 Å and (θ, ϕ) = (10°, 167°) are shown.

The selected structures at basin B are also consistent with the ^{13}C−^{15}N and ^{13}C−^{13}C distances measured by the rotational echo double resonance (REDOR) and rotational resonance (RR) experiments of MAS solid-state NMR spectroscopy (Table 2).[14] Especially, the I1[^{13}C′]−G5[^{15}N] distance of 6.0 Å was reproduced only by the structures in basin B with the extended conformation of N-terminal two residues. The distances in the α-helical structures on W3−L14 also agree with the other four experimental precise distances.

Selection of MP-X Backbone Structures Relative to the Membrane by the Dipolar Couplings between MP-X and Lipids. In a previous communication, we reported ^{13}C MAS NMR spectra for COXSHD whose signal intensities depend on distances between ^{1}H spins covalently bonding to ^{13}C spins in a peptide and X (^{2}H or ^{31}P) spins in phospholipids (Figure 3a).[15] We observed the COXSHD spectra for MP-X bound to liposomes composed of deuterated dimyristoylphosphatidylcholine (d_{62}-DPPC) and dimyristoylphosphatidylglycerol (d_{62}-DPPG) (4:1) at a probe temperature of 223 K at a magic-angle-spinning

dx.doi.org/10.1021/jp205290t |J. Phys. Chem. B 2011, 115, 9327–9336

frequency of 12.5 kHz. MP-X tightly binds to the lipid bilayers but does not disrupt the bilayer structure.[13] We estimated the depth and orientation of the peptide backbone in the bilayers by fitting simulated spectra to the experimental ones for the backbone (PDB: 2CZP) in the membranes.

Here, the COXSHD spectra of MP-X in a C^{α} region, 45−68 ppm, were calculated using the 762 MP-X molecules in basin B in order to evaluate the simulated peptide orientation and depth in the implicit membranes. The spectral simulation was based on the ^{1}H-demagnetization as a function of z, calculated with the distribution of ^{2}H and ^{31}P atoms in a lipid bilayer generated by molecular dynamics simulation of a DPPC bilayer system (Figure 3b).[15] We made experiments at the low temperature of 223 K to suppress the peptide dynamics which affects the effective dipolar couplings. We adopted the depth z in the DPPC bilayer system for calculating the spectra, instead of the depth z_{IM} in the implicit membrane for the REMD simulation. The peptide depth is given by the z coordinate of the center of mass of C^{α} nuclei in the backbone. The target function for the spectral fitting E is expressed as

$$E = \sqrt{\frac{\sum_i (S_{D,exp,i} - S_{D,sim,i})^2}{N\sigma_D^2} + \frac{\sum_i (S_{P,exp,i} - S_{P,sim,i})^2}{N\sigma_P^2}}$$

where S_i represents COXSHD signal intensity at data point i, N is the total number of spectral points, subscripts "D" and "P" denote ^{2}H- and ^{31}P-selective ^{1}H-demagnetization, and "exp" and "sim" stand for experimental and simulated spectra, respectively. We included the rms spectral noise σ_D and σ_P to minimize the effect of noise in spectra with different signal-to-noise (S/N) ratios. When $E \approx 1$, the difference between the experimental and simulated spectra is comparable to the spectral noise.

The target function E was minimal at a peptide depth of $z = 18.0 \pm 1.5$ Å for the structure and orientation at basin B, showing that the peptide main chain resided near the lipid headgroups as previously reported (Figure 3c).[15] We also examined the peptide orientation relative to the membranes by the spectral fitting. The orientation angles for the simulated conformations were distributed at $(\theta, \phi) = (16 \pm 10°, 168 \pm 12°)$, where θ and ϕ are tilt and rotation angles (Figure 3d,e). The lower $E \leq 1$ was observed around $(\theta, \phi) = (10°, 167°)$ at $z = 18.0$ Å. This peptide topology is clearly distinguishable from the others by the spectral pattern of COXSHD and $E > 1$ (Figure S4 in the Supporting Information). The α-helix of MP-X at basin B lay almost in the region $z_{IM} = 17.0 \pm 1.0$ Å corresponding to the implicit interfacial layer ($16.5 \leq z_{IM} \leq 21.5$ Å) shown in Figure 1a and Figure S1a in the Supporting Information, reflecting the amphiphilicity of the helix. Thus the depth z giving the ^{2}H and ^{31}P distribution used for the spectral fitting almost coincides with z_{IM} for the REMD simulation in the peptide position. The hydrophobic residues W3, I6, A10, L13, and L14 were located on the inside of the membrane, while the hydrophilic residues K4, K11, and K12 faced the aqueous region. A majority of structures in basin B satisfied the orientational constraint $5° < \theta < 20°$ given by the COXSHD spectra (Figure 3d). The backbone orientation is consistent with that determined in our preceding study.[15]

Selection of Side Chain Structures by the Heteronuclear Dipolar Couplings. We previously determined only the backbone structure of MP-X by solid-state NMR experiments.[14,15,28] In this study, we extracted information about the side chain structures in the lipid membranes from the side chain spectral regions of COXSHD spectra using the REMD simulation and spectral calculation. The side chain structures were generated by the 10-ns REMD simulation for the backbone structure at basin B with the orientation angles of $(\theta, \phi) = (10°, 167°)$ and $z_{IM} = 17$ Å in the interface region. The resulting 5000 structures sampled every 1 ps for 5−10-ns simulation time at 300 K were subjected to analysis. The target function E for the aliphatic side chain (0−45 ppm) and the indole ring (100−140 ppm) regions were calculated from the simulated structures placed at $z = 18$ Å, the depth with the minimal E value for the C^{α} region.

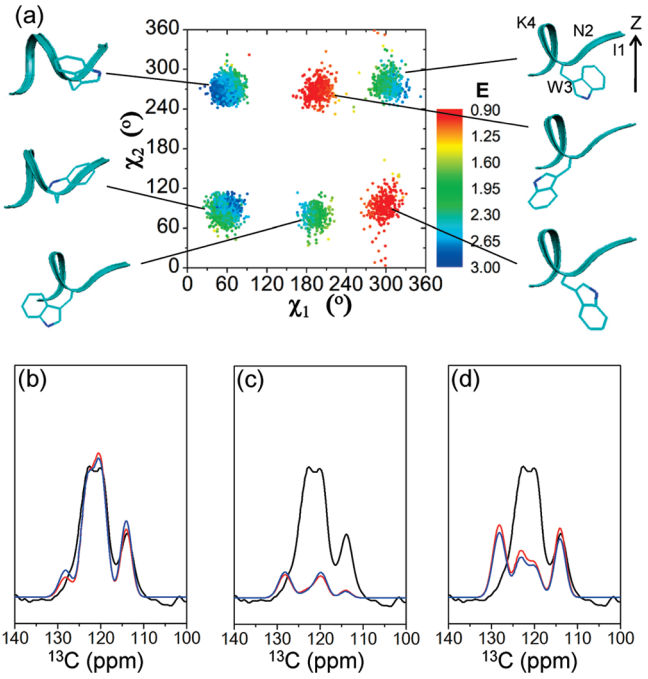

Figure 4. (a) Target function E for fitting the spectra in the region from 100 to 140 ppm depending on side chain torsion angles (χ_1, χ_2) of W3 in the REMD simulation. The representative side chain orientations of W3 were shown. The arrow indicates the membrane normal. (b−d) Observed (black) and simulated CO^{2}HSHD spectra for the indole ring with the torsion angles (χ_1, χ_2): (180°, 270°) for (b, red); (300°, 90°) for (b, blue); (180°, 90°) for (c, red); (300°, 270°) for (c, blue); (60°, 90°) for (d, red); (60°, 270°) for (d, blue).

Figure S5 in the Supporting Information shows correlations between the target function E and the side chain depth given by the center of mass. We found a strong correlation with the coefficient $r = 0.92$ between the W3 depth and E calculated for the region 100−140 ppm. Figure 4a shows E as a function of side chain torsion angles χ_1 and χ_2 for W3 in the simulation. The torsion angles were classified into six rotamers with $(\chi_1, \chi_2) = (60°, 90°)$, $(60°, 270°)$, $(180°, 90°)$, $(180°, 270°)$, $(300°, 90°)$, and $(300°, 270°)$. This torsion angle distribution was consistent with the side chain rotamer library, indicating the correct sampling in the side chain conformational space under the CHARMM force field and the implicit membrane/solvent model.[29] The best spectral fit was observed only at $(\chi_1, \chi_2) = (180°, 270°)$ and $(300°, 90°)$ (Figure 4b−d). Two orientations, however, could not be distinguished. They yield almost the same COXSHD spectra because the rings are symmetric about the membrane normal. These angles indicate that the indole ring was inserted into the lipid membranes with its long axis running almost parallel to the membrane normal and the polar nitrogen

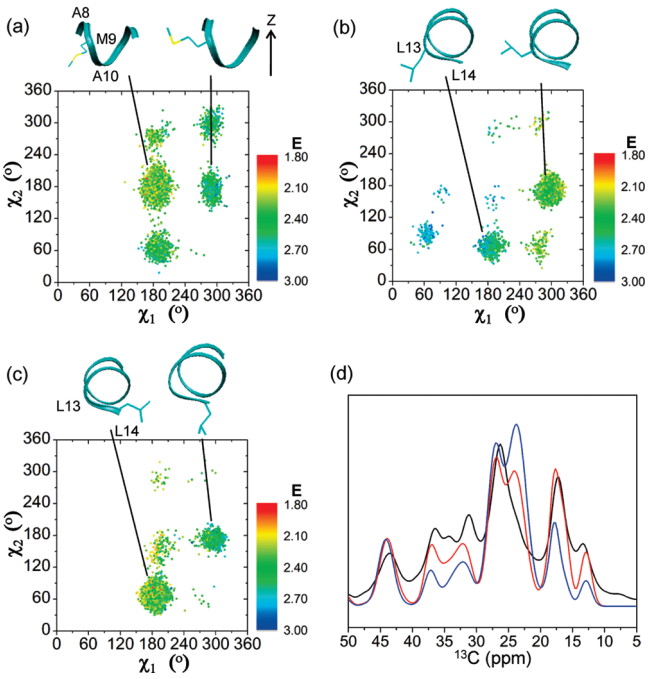

Figure 5. Target function E for the spectral region from 0 to 45 ppm as a function of side chain torsion angles for M9 (a), L13 (b), and L14 (c). (d) Observed (black), best-fit simulated (red), and worst-fit simulated (blue) CO^2HSHD spectra.

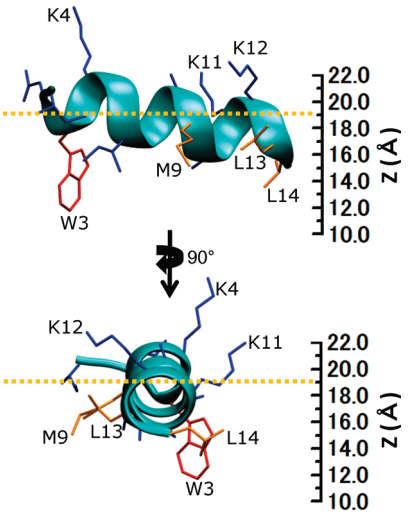

Figure 6. Structure of MP-X in lipid bilayers. The level at the maximum of the phosphorus density is shown by yellow dotted lines. Hydrogen atoms are omitted. The side chains are color-coded according to the correlation coefficient r between the COXSHD target function E and the side chain orientations (Figure S5 in the Supporting Information): red for $|r| > 0.9$; orange for $|r| > 0.5$; blue for $|r| \leq 0.5$.

atom facing toward the hydrophilic region as shown by the rings corresponding to the red basins in Figure 4a. The result agrees with the previous studies on small compounds where indole rings prefer to be localized at the membrane interface and their plane oriented parallel to lipid chains due to steric restrictions.[30,31] These six rotamers may appear in the REMD simulation because of the absence of strong repulsive interactions between the lipid and the peptide molecules in the implicit membranes.

The side chains of M9, L13, and L14 show the correlations between E and the depth with $r = 0.56$, -0.75, and -0.56, respectively (Figure S5 in the Supporting Information). The side chain torsion angles were also analyzed as shown in Figure 5. Residues M9, L13, and L14 preferred the angles $(\chi_1, \chi_2) = (180°, 180°)$, $(300°, 180°)$, and $(180°, 60°)$, respectively. The M9 side chain was oriented toward the hydrophobic part of the membrane, while L13 and L14 side chains mainly resided on the side of the helix not below that. The relatively poor spectral fit with $E > 1$ implies heterogeneity of side chain structures even at the low experimental temperature of 223 K, while the better fit with lower E for the backbone and W3 side chain indicates well-defined structures. Leucine side chain motions of membrane proteins are restricted at a temperature below a phase transition point of lipids, and only methyl rotation dominates ^2H spectra due to quadrupolar couplings.[32,33] Thus, there should be no major motional averaging on the aliphatic side chains.

We detected no significant correlations between the spectral fit and the depth of the side chains for I1 and I6, probably owing to the small displacements along the z-axis (Figure S5 in the Supporting Information). Only one χ_1 rotamer centered at 300° was allowed especially for I6 because of the steric interactions with the α-helical backbone. In contrast, K4, K11, and K12 side chain positions did not affect the spectral fit despite their relatively large displacements. This is because the polar Lys residues were located in the hydrophilic part of the membranes where the demagnetization curve for ^2H reached zero (Figure 3b). This side chain structure is illustrated in Figure 6. This structure is corroborated by the COXSHD spectra in the Lys side chain region 30−35 ppm, which indicated that the structure in Figure 6 gave the helix rotation angle ϕ of 170° ± 8° in agreement with 167° determined from the C^α spectral region (Figure S6 in the Supporting Information). The REMD simulation also showed that the cationic $-NH_3^+$ groups were positioned in the aqueous and the dielectric boundary regions whereas the methylene chain remained in more hydrophobic regions.[34] Note that the side chain orientations could not be determined only by the ^{31}P-depolarized spectra with a lower S/N ratio.

DISCUSSION

Structure of MP-X in Lipid Bilayers. The MP-X molecular model in the lipid bilayer in Figure 6 summarizes all the backbone and side chain orientations and structures described above. This structure shows that the N-terminal lies closer to the water layer than the C-terminal. The N-terminal part contains the hydrophilic side chain at N2 and cationic NH_3^+ at I1. The W3 backbone is allowed to reside in the interface level by extending the hydrophobic side chain into the inside of the membrane as shown by red dots in Figure 4 corresponding to the conformers. This agrees with the result that the W3 residue of membrane-bound MP-X was in hydrophobic environments as revealed by a blue shift and an intensity increase in the fluorescence spectrum.[13] The C-terminal part contains the hydrophobic side chains at L13 and L14 together with the amide suppressing the carboxyl charge. Insertion of this C-terminal into the lipid hydrophobic domain is limited by the cationic NH_3^+ of K11 and K12 anchoring at the hydrophobic interface level. The extended methylene side chains allowed the backbone to stay in the hydrophobic interface. Binding to lipid vesicles potentiates the G protein stimulating activity of mastoparans.[35] The cationic side chains presented on the surface of lipid bilayers are suited for

dx.doi.org/10.1021/jp205290t |J. Phys. Chem. B 2011, 115, 9327–9336

the recognition by G proteins in signal transduction.[36] These side chain orientations having charged and hydrophobic atomic groups should primarily restrict the tilt angle to about 15°. Thus the tilt angle can be altered by the side chain orientations within about 15°.

Validation of the REMD Simulations with the Implicit Membrane/Solvent Model. In this study, we performed the REMD simulations of MP-X with the implicit membrane/solvent model. The structure with the backbone rmsd of less than 1.0 Å from the NMR structure was found at the stable basin in the energy landscape. In addition, the MD simulation reproduced the location of the peptide in the membranes experimentally determined. Thus the present REMD simulation was capable of predicting the backbone structure in the membranes without using experimental constraints. This simulation with the implicit membrane/solvent model has several advantages. First, the calculation does not require expensive computational costs, because a large number of solvent and lipid molecules surrounding the proteins are not necessary. All-atom systems for reliable MD simulation of peptides would need a number of atoms about 50 times larger than the implicit membrane systems. Second, the replica exchange method can efficiently search the large structural space for the global minimum without a system getting trapped in local minima. So far, the MD simulations with implicit membrane/solvent models have been used for a number of membrane proteins and peptides with functions such as antimicrobial properties, channels, amyloid formation, and signal regulation, e.g., melittin, protegrin-1, glycopholin A, amyloid β-protein, and phospholamban.[4−6,37−40] Most simulations are in agreement with experimental observations for the structures of the proteins in membranes. In addition, fully extended polypeptides folded into the nativelike structures during the REMD simulations.[4,5,40] The above systems included polypeptides with lengths from 16 to 55 residues forming α-helixes, β-sheets, and hairpins at membrane-bound and -integrated states. This implies that the structure determination employed here is applicable to a wide range of membrane protein and peptide systems. Moreover, our results revealed that the combined use of experimental data such as chemical shifts and dipolar couplings enhances the accuracy of the determination by the REMD simulations.

The implicit membrane model, however, has several limitations. Because lipid bilayers are treated as a low dielectric slab, we may not deal with events relevant to deformation of the membrane structures such as membrane fusion and the heterogeneity in the membrane *xy*-plane such as interactions with specific lipid molecules, e.g., PH domains which specifically recognize phosphatidylinositols.[41] The limitation of the force field was reported in the refinement of protein structures especially for long and flexible loops mainly due to the inaccuracy of the nonpolar solvation term in the continuum solvent model.[10,42]

Determination of Membrane Peptide Structures by Limited Experimental Data. Here, we selected the correct molecular conformation of the membrane-bound peptide from the simulated conformational ensemble by using the ^{13}C chemical shifts. The correct structures were discriminated from the others by the difference between the experimental and predicted chemical shifts using SHIFTX and SPARTA. The $^{13}C^{\alpha}$ chemical shifts alone were sufficient for the selection of the structures. Consequently, we obtained the same MP-X structures as the NMR structure that was determined independently using the distances obtained from the REDOR and RR experiments and the dihedrals predicted by the TALOS program from the chemical shifts of C^{α}, C^{β}, C′, and ^{15}N nuclei.[14,43] We previously performed simulated-annealing spectral fitting for MAS NMR by molecular dynamics calculation with simplified potentials in CNS.[11] Although this method enabled the automatic signal assignments, it was not sufficient for obtaining the correct structure of membrane-bound MP-X.

We obtained the information of the side chain and backbone locations in the lipid bilayers from the intermolecular dipolar couplings between lipids and peptides. The distance constraints were extracted from the one-dimensional spectra of the uniformly isotope labeled peptide by the REMD-derived structures and the simulations of COXSHD spectra. The analysis by the spectral fitting provided the structural parameters even from broad signals consisting of unresolved 14 $^{13}C^{\alpha}$ resonances (Figure 3e,f and Figure S4 in the Supporting Information). The present method has higher resolution for residues around the interface layer especially in contact with lipid acyl chains. The depth, tilt angle, and rotation angle of the MP-X backbone were estimated with accuracy ±1.5 Å, ± 8°, and ±12°, respectively, from the criteria, $E \leq 1$. The side chain orientations were specified with higher precision for W3, M9, L13, and L14 because these orientations give rise to dipolar couplings between the side chain protons and the deuterons in the lipids. The experimental backbone and side chain locations confirmed the accuracy of MD simulations as described under Results.

This method for probing peptide location in the bilayers with the intermolecular dipolar couplings has several advantages. Since the structural restraints are obtained from distances through dipolar couplings, this method provides the peptide depth, which cannot be obtained from the angles obtained from NMR of oriented systems such as correlation between ^{15}N chemical shift anisotropies and NH dipolar couplings.[44] Chemical modifications and addition of paramagnetic ions also provide the information on peptide location in the membranes, but these methods may perturb the conformations and dynamics of the systems.[45,46] In contrast, our method for the membrane binding mode was performed without them. The distance between bulk water layer and peptides in the membrane measurement can be measured by $^{1}H-^{1}H$ spin diffusion.[47] This method may supplement the structural constraints obtained by our methods by providing long distances over 10 Å, but with precisions lower than 1.5 Å for the present analysis because of the complexity of the spin diffusion in the membrane protein systems.

The present strategy can be applied to larger membrane protein complex systems. The analysis of complex systems should be facilitated by chemical shifts other than C^{α}, C^{β}, and C′ and spectra for intermolecular interactions such as for protein−protein, protein−ligand, protein−water, and protein−lipid.[48−52] Dipolar interactions can be derived from the spectra for intermolecular interactions by the spectral simulations as performed here. However, the reduction in further spectral resolution due to further signal overlap would lead to lower structural resolution. In addition, better initial model conformations would be required for the REMD simulation because it is still difficult to find the native conformation in the trajectories calculated from initial fully extended structure.

CONCLUSIONS

We have demonstrated that the combination of the REMD simulation with the implicit membrane/solvent model and the solid-state NMR spectral simulations are useful for determining

the peptide structure and location in the lipid bilayers. The REMD simulation and solid-state NMR spectroscopy are complementary to each other. Solid-state NMR improved the accuracy of the structure provided by the REMD simulation. We selected the structures from the simulation using the experimental ^{13}C chemical shifts and COXSHD spectra giving heteronuclear dipolar couplings. On the other hand, the REMD simulation supplemented the structural constraints obtainable from the solid-state NMR spectra. Only the $^{13}C^{\alpha}$ chemical shifts and the one-dimensional dipolar spectra were enough to determine the backbone and side chain structure of MP-X relative to the lipid bilayers. The present strategy shed light on structure determination of membrane proteins from a limited amount of structural information such as unresolved solid-state NMR spectra of fully isotope labeled molecules.

■ ASSOCIATED CONTENT

Supporting Information. Trajectories of the REMD simulations at 300 K; chemical shift predictions for C^{β} and C' nuclei; COXSHD spectral simulations for MP-X side chain conformations. This material is available free of charge via the Internet at http://pubs.acs.org.

■ AUTHOR INFORMATION

Corresponding Author

*E-mail: tfjwr@protein.osaka-u.ac.jp.

Present Addresses

[§]Bioorganic Research Insititute, Suntory Foundation for Life Sciences, 1-1-1Wakayamadai, Shimamoto, Mishima, Osaka 618-8503, Japan.

■ ACKNOWLEDGMENT

This work was supported by funding from the Targeted Proteins Research Program and KAKENHI of the Ministry of Education, Culture, Sports, Science and Technology of Japan.

■ REFERENCES

(1) Hong, M. *Structure* **2006**, *14*, 1731–1740.
(2) McDermott, A. *Annu. Rev. Biophys.* **2009**, *38*, 385–403.
(3) Sugita, Y.; Okamoto, Y. *Chem. Phys. Lett.* **1999**, *314*, 141–151.
(4) Im, W.; Brooks, C. L., III. *J. Mol. Biol.* **2004**, *337*, 513–519.
(5) Im, W.; Brooks, C. L., III. *Proc. Natl. Acad. Sci. U.S.A.* **2005**, *102*, 6771–6776.
(6) Im, W.; Feig, M.; Brooks, C. L., III. *Biophys. J.* **2003**, *85*, 2900–2918.
(7) Im, W.; Lee, M. S.; Brooks, C. L., III. *J. Comput. Chem.* **2003**, *24*, 1691–1702.
(8) Shen, Y.; Lange, O.; Delaglio, F.; Rossi, P.; Aramini, J. M.; Liu, G.; Eletsky, A.; Wu, Y.; Singarapu, K. K.; Lemak, A.; Ignatchenko, A.; Arrowsmith, C. H.; Szyperski, T.; Montelione, G. T.; Baker, D.; Bax, A. *Proc. Natl. Acad. Sci. U.S.A.* **2008**, *105*, 4685–4690.
(9) Lee, J.; Chen, J.; Brooks, C. L., III; Im, W. *J. Magn. Reson.* **2008**, *193*, 68–76.
(10) Chen, J.; Im, W.; Brooks, C. L., III. *J. Am. Chem. Soc.* **2004**, *126*, 16038–16047.
(11) Matsuki, Y.; Akutsu, H.; Fujiwara, T. *J. Biomol. NMR* **2007**, *38*, 325–339.
(12) Schwarz, G.; Blochmann, U. *FEBS Lett.* **1993**, *318*, 172–176.
(13) Matsuzaki, K.; Yoneyama, S.; Murase, O.; Miyajima, K. *Biochemistry* **1996**, *35*, 8450–8456.
(14) Todokoro, Y.; Yumen, I.; Fukushima, K.; Kang, S. W.; Park, J. S.; Kohno, T.; Wakamatsu, K.; Akutsu, H.; Fujiwara, T. *Biophys. J.* **2006**, *91*, 1368–1379.
(15) Harada, E.; Todokoro, Y.; Akutsu, H.; Fujiwara, T. *J. Am. Chem. Soc.* **2006**, *128*, 10654–10655.
(16) Brooks, B. R.; Bruccolei, R. E.; Olafson, B. D.; States, D. J.; Swaminathan, S.; Karplus, M. *J. Comput. Chem.* **1983**, *4*, 187–217.
(17) MacKerell, A. D.; Bashford, D.; Bellott, M.; Dunbrack, R. L.; Evanseck, J. D.; Field, M. J.; Fischer, S.; Gao, J.; Guo, H.; Ha, S.; Joseph-McCarthy, D.; Kuchnir, L.; Kuczera, K.; Lau, F. T. K.; Mattos, C.; Michnick, S.; Ngo, T.; Nguyen, D. T.; Prodhom, B.; Reiher, W. E.; Roux, B.; Schlenkrich, M.; Smith, J. C.; Stote, R.; Straub, J.; Watanabe, M.; Wiorkiewicz-Kuczera, J.; Yin, D.; Karplus, M. *J. Phys. Chem. B* **1998**, *102*, 3586–3616.
(18) Ryckaert, J. P.; Ciccotti, G.; Berendsen, H. J. C. *J. Comput. Phys.* **1977**, *23*, 327–341.
(19) Hoover, W. G. *Phys. Rev. A* **1985**, *31*, 1695–1697.
(20) Feig, M.; MacKerell, A. D.; Brooks, C. L. *J. Phys. Chem. B* **2003**, *107*, 2831–2836.
(21) Frishman, D.; Argos, P. *Proteins: Struct., Funct., Genet.* **1995**, *23*, 566–579.
(22) Kameda, T.; Takada, S. *Proc. Natl. Acad. Sci. U.S.A.* **2006**, *103*, 17765–17770.
(23) Ikeda, K.; Galzitskaya, O. V.; Nakamura, H.; Higo, J. *J. Comput. Chem.* **2003**, *24*, 310–318.
(24) Neal, S.; Nip, A. M.; Zhang, H.; Wishart, D. S. *J. Biomol. NMR* **2003**, *26*, 215–240.
(25) Shen, Y.; Bax, A. *J. Biomol. NMR* **2007**, *38*, 289–302.
(26) Feller, S. E.; Yin, D.; Pastor, R. W.; MacKerell, A. D., Jr. *Biophys. J.* **1997**, *73*, 2269–2279.
(27) Seidel, K.; Etzkorn, M.; Schneider, R.; Ader, C.; Baldus, M. *Solid State Nucl. Magn. Reson.* **2009**, *35*, 235–242.
(28) Fujiwara, T.; Todokoro, Y.; Yanagishita, H.; Tawarayama, M.; Kohno, T.; Wakamatsu, K.; Akutsu, H. *J. Biomol. NMR* **2004**, *28*, 311–325.
(29) Lovell, S. C.; Word, J. M.; Richardson, J. S.; Richardson, D. C. *Proteins* **2000**, *40*, 389–408.
(30) Esbjorner, E. K.; Caesar, C. E.; Albinsson, B.; Lincoln, P.; Norden, B. *Biochem. Biophys. Res. Commun.* **2007**, *361*, 645–650.
(31) Yau, W. M.; Wimley, W. C.; Gawrisch, K.; White, S. H. *Biochemistry* **1998**, *37*, 14713–14718.
(32) Keniry, M. A.; Kintanar, A.; Smith, R. L.; Gutowsky, H. S.; Oldfield, E. *Biochemistry* **1984**, *23*, 288–298.
(33) Tiburu, E. K.; Karp, E. S.; Dave, P. C.; Damodaran, K.; Lorigan, G. A. *Biochemistry* **2004**, *43*, 13899–13909.
(34) Strandberg, E.; Killian, J. A. *FEBS Lett.* **2003**, *544*, 69–73.
(35) Higashijima, T.; Burnier, J.; Ross, E. M. *J. Biol. Chem.* **1990**, *265*, 14176–14186.
(36) Kusunoki, H.; Wakamatsu, K.; Sato, K.; Miyazawa, T.; Kohno, T. *Biochemistry* **1998**, *37*, 4782–4790.
(37) Sayyed-Ahmad, A.; Kaznessis, Y. N. *PLoS One* **2009**, *4*, e4799.
(38) Sayadi, M.; Tanizaki, S.; Feig, M. *Biophys. J.* **2010**, *98*, 805–814.
(39) Miyashita, N.; Straub, J. E.; Thirumalai, D.; Sugita, Y. *J. Am. Chem. Soc.* **2009**, *131*, 3438–3439.
(40) Miyashita, N.; Straub, J. E.; Thirumalai, D. *J. Am. Chem. Soc.* **2009**, *131*, 17843–17852.
(41) Lemmon, M. A. *Nat. Rev. Mol. Cell Biol.* **2008**, *9*, 99–111.
(42) Chen, J.; Brooks, C. L., III. *Proteins* **2007**, *67*, 922–930.
(43) Cornilescu, G.; Delaglio, F.; Bax, A. *J. Biomol. NMR* **1999**, *13*, 289–302.
(44) Opella, S. J.; Marassi, F. M. *Chem. Rev.* **2004**, *104*, 3587–3606.
(45) Grobner, G.; Glaubitz, C.; Watts, A. *J. Magn. Reson.* **1999**, *141*, 335–339.
(46) Tucker, M. J.; Getahun, Z.; Nanda, V.; DeGrado, W. F.; Gai, F. *J. Am. Chem. Soc.* **2004**, *126*, 5078–5079.
(47) Gallagher, G. J.; Hong, M.; Thompson, L. K. *Biochemistry* **2004**, *43*, 7899–7906.
(48) Etzkorn, M.; Bockmann, A.; Lange, A.; Baldus, M. *J. Am. Chem. Soc.* **2004**, *126*, 14746–14751.

(49) Kiihne, S. R.; Creemers, A. F.; de Grip, W. J.; Bovee-Geurts, P. H.; Lugtenburg, J.; de Groot, H. J. *J. Am. Chem. Soc.* **2005**, *127*, 5734–5735.
(50) Toke, O.; Maloy, W. L.; Kim, S. J.; Blazyk, J.; Schaefer, J. *Biophys. J.* **2004**, *87*, 662–674.
(51) Ader, C.; Schneider, R.; Seidel, K.; Etzkorn, M.; Becker, S.; Baldus, M. *J. Am. Chem. Soc.* **2009**, *131*, 170–176.
(52) Feller, S. E.; Venable, R. M.; Pastor, R. W. *Langmuir* **1997**, *13*, 6555–6561.